ISSN 1674-1056
http://cpb.iphy.ac.cn
http://iopscience.iop.org/cpb
中国物理 B
Chinese Physics
中国物理
Chinese Physics B

# Influence of additives on the magnetic damping constant of CoIr soft magnetic thin films with negative magnetocrystalline anisotropy

Tianyong Ma(马天勇), Zhi Luo(罗智), Zhiwei Li(李志伟), Liang Qiao(乔亮), Tao Wang(王涛), Fashen Li(李发伸)

**Citation:**Chin. Phys. B . 2019, 28(5): 057505. **doi:** 10.1088/1674-1056/28/5/057505
Journal homepage: http://cpb.iphy.ac.cn; http://iopscience.iop.org/cpb

**What follows is a list of articles you may be interested in**

---

## Interplay of Rashba effect and spin Hall effect in perpendicular Pt/Co/MgO magnetic multilayers

Yun-Chi Zhao(赵云驰), Guang Yang(杨光), Bo-Wen Dong(董博闻), Shou-Guo Wang(王守国), Chao Wang(王超), Young Sun(孙阳), Jing-Yan Zhang(张静言), Guang-Hua Yu(于广华)
Chin. Phys. B . 2016, 25(7): 077501. **doi:** 10.1088/1674-1056/25/7/077501

## Effects of oxidation of $DyH_3$ in Nd-Fe-B sintered magnets

Yan Gao-Lin, Fang Zhi-Hao
Chin. Phys. B . 2015, 24(10): 107503. **doi:** 10.1088/1674-1056/24/10/107503

## Shape-manipulated spin-wave eigenmodes of magnetic nanoelements

Zhang Guang-Fu, Li Zhi-Xiong, Wang Xi-Guang, Nie Yao-Zhuang, Guo Guang-Hua
Chin. Phys. B . 2015, 24(9): 097503. **doi:** 10.1088/1674-1056/24/9/097503

## Room-temperature ferromagnetism with high magnetic moment in Cu-doped AlN single crystal whiskers

Jiang Liang-Bao, Liu Yu, Zuo Si-Bin, Wang Wen-Jun
Chin. Phys. B . 2015, 24(2): 027503. **doi:** 10.1088/1674-1056/24/2/027503

## Magnetic field control of ferroelectric polarization and magnetization of $LiCu_2O_2$ compound

Qi Yan, Du An
Chin. Phys. B . 2014, 23(8): 087502. **doi:** 10.1088/1674-1056/23/8/087502

---

# Influence of additives on the magnetic damping constant of CoIr soft magnetic thin films with negative magnetocrystalline anisotropy*

Tianyong Ma(马天勇), Zhi Luo(罗智), Zhiwei Li(李志伟)†, Liang Qiao(乔亮), Tao Wang(王涛)‡, and Fashen Li(李发伸)

*Key Laboratory for Magnetism and Magnetic Materials of the Ministry of Education, Key Laboratory for Special Functional Materials and Structure Design of the Ministry of Education, Lanzhou University, Lanzhou 730000, China*

(Received 10 December 2018; revised manuscript received 5 March 2019; published online 8 April 2019)

The oriented $(CoIr)_{100-x}P_x$ ($P$ = B, Ni, and $SiO_2$) soft magnetic films are prepared. Their morphology is measured using transmission electron microscopy (TEM), and reveals that these films exhibit good crystallinity and high degree of the $c$-axis orientation. The magnetic properties are thoroughly investigated as a function of doping $x$. Our results show that all of these films possess negative magnetocrystalline anisotropy as required by possible applications. Both the intrinsic and extrinsic contributions are considered to interpret the broadening of the ferromagnetic resonance spectral linewidth. The intrinsic Gilbert damping is identified as the main cause of the linewidth broadening, while the extrinsic part originating from inhomogeneities only plays a minor role. More interestingly, our results show that the damping constant can be controlled by using the doping method.

**Keywords:** magnetic damping constant additives, negative magnetocrystalline anisotropy

**PACS:** 75.40.Gb, 76.30.Lh, 75.50.–y **DOI:** 10.1088/1674-1056/28/5/057505

## 1. Introduction

The damping of precession is a critical issue in high frequency magnetism, which can be described by the damping constant $\alpha$ in various magnetic systems.[1,2] The $\alpha$ determines the switching time of the magnetization for ultra-high frequency devices. For example, in high-frequency magnetic recording, the switching time strongly depends on $\alpha$ and the magnetization reversal is faster when the damping constant is appropriate.[3] The Gilbert damping constant defined as $\alpha\gamma M_s$ is proportional to the critical current density $J_c$ in spin-transfer-torque devices, where $\gamma$ is the gyromagnetic ratio, and $M_s$ is the saturation magnetization.[4] Therefore, it is crucial to understand and control the damping constant for practical applications. Many theoretical studies have been carried out in an effort to understand the origin of the damping constant.[5–7] It is well-known that $\alpha$ contains both intrinsic and extrinsic contributions. The intrinsic part largely depends on the fundamental properties such as $M_s$ and spin–orbit coupling, while the extrinsic part is generally explained by the defect-induced two magnon mode and/or the local resonance mode, both of which are associated with magnetic inhomogeneities within the material.[8] In particular, much attention has been focused on the control of $\alpha$ using various methods, such as doping with rare earth or other transition metal elements.[9,10] For example, Rantschler *et al.* and Fassbender *et al.* reported the variation of $\alpha$ in 3d, 4d, and 5d transition metal doped FeNi films and the increase of the damping constant in permalloy films with the increase of Cr-doping, respectively.[11,12] More recently, Guo *et al.* have reported that the rare-earth Gd doping reduces the magnetic damping constant of FeCo films as probed by ferromagnetic resonance (FMR).[4]

In our previous work, the damping constant of CoIr films has been investigated thoroughly with thickness, substrate temperature, and Ir content.[13] CoIr films with a certain Ir content exhibit strong negative magnetocrystalline anisotropy, which means that the $c$-plane of the hcp-CoIr crystal is the easy magnetization plane and the $c$-axis is the corresponding hard axis.[14] The properties enhance the high frequency magnetic properties and the critical film thickness for the Néel type domain wall changing into Bloch type, and strictly restrict the magnetic moments in-plane of micrometer thick soft magnetic thin films (SMTFs).[15,16] Recently, the reduction of magnetic damping constant in Rh-incorporated CoIr system has been reported.[17] It is also reported that the doping elements B[18] and $SiO_2$[19] have an effect on soft magnetic properties of CoIr system. To understand the effects on the damping constant and gain control of the magnetic damping behavior, we prepared oriented hcp-CoIr thin films with different additives of B, Ni, and $SiO_2$. We have studied the effects of these additives on the damping constant by using ferromagnetic resonance.

## 2. Experiment

The layer structure of the films prepared by direct current (DC) magnetron sputtering was substrate/Ti/Au/$(CoIr)_{100-x}P_x$

*Project supported by the National Natural Science Foundation of China (Grant Nos. 11574122 and 11704167) and the Fundamental Research Funds for the Central Universities, China (Grant Nos. lzujbky-2017-k20 and lzujbky-2017-31).

†Corresponding author. E-mail: zweili@lzu.edu.cn

‡Corresponding author. E-mail: wtao@lzu.edu.cn

© 2019 Chinese Physical Society and IOP Publishing Ltd 

($P$ = B, Ni, and $SiO_2$), as shown in Fig. 2(a). The Si wafer with surface oxidation was used as a substrate. The amorphous Ti layer of 3 nm provided an flat and clean surface that assists the oriented growth of the Au layer with (111) plane parallel to the thin film, and the oriented Au layer of 10 nm was used to induce the oriented growth of $(CoIr)_{100-x}P_x$ soft magnetic layer with its $c$-axis normal to the film surface. Both Ti layer and Au seed layer were made with pure Ar at a pressure of 0.25 Pa, then the $(CoIr)_{100-x}P_x$ magnetic layers were deposited on the seed layer with 0.3 Pa Ar gas. Both the Co target with five Ir chips and the corresponding $P$ target were used. The substrate from the targets about 15 cm away was mounted on a turntable, which was rotated about its central axis. The in-plane uniaxial anisotropy can be induced by placing the substrates slightly off-centered on the turntable. The contents of $P$ can be varied by changing the gun power while keeping the CoIr gun power at 60 W. In the following discussion, as shown in Table 1, the studied samples will be denoted as $Px$ corresponding to the film with $(CoIr)_{100-x}P_x$ magnetic layer.

**Table 1.** Naming method for $(CoIr)_{100-x}P_x$ films where $P$ denotes B, Ni, or $SiO_2$.

| CoIr | $P/x$ | Naming method |
|---|---|---|
| $Co_{79}Ir_{21}$ | $B/x = 0$, 3, 6.5, 8.7, 10.8 | B$x$ |
| $Co_{79}Ir_{21}$ | $Ni/x = 0$, 3.4, 5.3, 7.1, 10.6 | Ni$x$ |
| $Co_{79}Ir_{21}$ | $SiO_2/x = 0$, 3.5, 5.2, 7, 8.7 | SiO$x$ |

## 3. Theoretical fitting

The FMR measurements are performed in a Joel electron paramagnetic resonance spectrometer at 9 GHz in a scanning DC magnetic field (0–20 kOe). The magnetic field is applied by an electromagnet, and the sample is fixed onto a 0–360 rotatable quartz rod and a goniometer is used to control the rotation of the quartz rod. For magnetic thin films, FMR based on the approximation of spatially uniform precession of the magnetization over the whole film is analyzed in the following. Figure 1 shows the coordinate system used for the FMR measurements and data analysis. The film plane is in the $x$–$y$ plane and the film normal direction is parallel to the $z$-axis. $M_s$, $\theta_M$, and $\phi_M$ are amplitude, polar, and azimuthal angles of the magnetization vector $\boldsymbol{M}$. The static field $\boldsymbol{H}$ is applied in plane with an azimuthal angle $\phi_H$ and the small microwave magnetic field $h$ is applied along the $z$-axis. Then, the total magnetic free energy per unit volume of the film is given by the following equation:[20]

$$\begin{aligned} F &= -HM\sin\theta_M\cos(\phi_H-\phi_M)+(2\pi M^2-K_{\rm grain})\cos^2\theta_M \\ &\quad -K_{\rm u}\sin^2\theta_M\cos^2(\phi_M-\phi_{\rm u}), \end{aligned} \tag{1}$$

where $\phi_{\rm u}$ is the angle between the easy axis of the film and the $x$-axis, $K_{\rm u}$ is the in-plane uniaxial anisotropy (IPUA), and $K_{\rm grain}$ is the negative magnetocrystalline anisotropy (NMA). The first, second, and third terms in Eq. (1) represent the Zeeman energy, demagnetization plus NMA energy, and the IPUA energy, respectively.

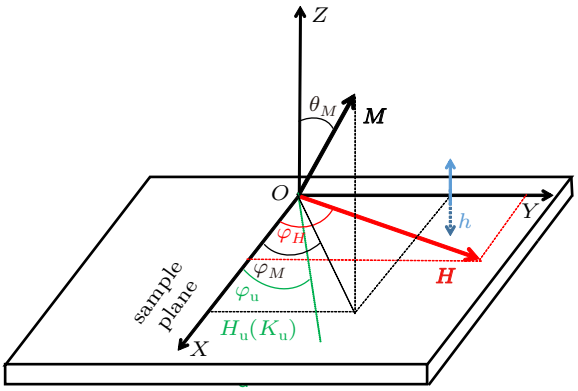



**Fig. 1.** The coordinate system used for measurements and data analysis of the FMR spectra.

Solving the Landau–Lifshitz–Gilbert (LLG) equation with weak damping, the standard condition for resonance becomes

$$\left(\frac{\omega}{\gamma}\right)^2=\frac{1}{M^2\sin^2\theta_M}\left[\left(\frac{\partial^2F}{\partial\theta_M^2}\right)\left(\frac{\partial^2F}{\partial\phi_M^2}\right)-\left(\frac{\partial^2F}{\partial\theta_M\partial\phi_M}\right)^2\right], \tag{2}$$

where $\omega$ is the angular frequency of $\sim 18\pi$ GHz and $F$ is the free energy. The resonance field as a function of field orientation $\phi_H$ can be expressed by the following equation:[16]

$$\begin{aligned} \left(\frac{\omega}{\gamma}\right)^2 &= \left[{\rm H}_\theta+H_{\rm u}\cos^2(\phi_0-\phi_{\rm u})+H_{\rm r}\cos(\phi_0-\phi_H)\right] \\ &\quad\times\left[H_{\rm u}\cos(2\phi_0-2\phi_{\rm u})+H_{\rm r}\cos(\phi_0-\phi_H)\right], \end{aligned} \tag{3}$$

where $H_{\rm r}$ is the resonance field, $\phi_0$ is the value of $\phi_M$ at the equilibrium position, $H_{\rm u}=2K_{\rm u}/M_{\rm s}$ is the in-plane uniaxial anisotropy field, and $H_\theta=4\pi M_{\rm s}-H_{\rm grain}$ ($H_{\rm grain}=2K_{\rm grain}/M_{\rm s}$) is the total out-of-plane anisotropy field. When the condition $H_\theta \gg H_{\rm u}$, $H_{\rm r}$ is fulfilled, and the resonance field can then be expressed as

$$\begin{aligned} H_{\rm r} &= \left(\frac{\omega}{\gamma}\right)^2[H_\theta\cos(\phi_0-\phi_H)]^{-1} \\ &\quad -H_{\rm u}\cos(2\phi_0-2\phi_{\rm u})\cos^{-1}(\phi_0-\phi_H). \end{aligned} \tag{4}$$

Furthermore, the following equilibrium equation of the magnetization vector is required:

$$2H_{\rm r}\sin(\phi_H-\phi_0)=H_{\rm u}\sin(2\phi_0-2\phi_{\rm u}). \tag{5}$$

For the spectral linewidth, we have considered the following expression:[21]

$$\begin{aligned} \Delta H &= \frac{1}{\sqrt{3}}\frac{\alpha}{M}\left(\frac{\partial^2F}{\partial\theta_M^2}+\frac{1}{\sin^2\theta}\frac{\partial^2F}{\partial\phi_M^2}\right)\left|\frac{{\rm d}(\omega/\gamma)}{{\rm d}H_{\rm r}}\right|^{-1} \\ &\quad +\frac{1}{\sqrt{3}}\left|\frac{\partial H_{\rm r}}{\partial\phi_{\rm u}}\right|\Delta\phi_{\rm u}+\Delta H(0). \end{aligned} \tag{6}$$

The first term represents the homogeneous broadening due to intrinsic contributions. The second term is the contribution from the angular dispersion of the easy axis $\Delta\phi_u$ originating from inhomogeneities due to defects and/or internal stress. $\Delta H(0)$ is a frequency and angle independent term that is related to thermal history, as well as the preparation process of the material. Considering the conditions of $H_\theta \gg H_u$ and $\phi_u = 0$, the expression for linewidth can be obtained

$$\Delta H \cong \frac{2}{\sqrt{3}}\frac{\alpha}{\gamma}\frac{\omega}{|\cos(\phi_H-\phi_0)|}+\frac{2H_u}{\sqrt{3}}\left|\frac{\sin 2\phi_0}{\cos(\phi_H-\phi_0)}\right|\Delta\phi_u + \Delta H(0). \quad (7)$$

We have performed numerical fitting to match the experimental data for each sample with Eqs. (4)–(7) by using MATLAB program to obtain the damping constant $\alpha$ as well as $\Delta\phi_u$ and $\Delta H$.

## 4. Results and discussion

In Fig. 2(b), we present the x-ray diffraction (XRD) patterns for SiO8.7, Ni7.1, and B8.7 films. Only two diffraction peaks can be observed for all the samples corresponding to the Au-seed layer (111)-plane and hcp-$(CoIr)_{100-x}P_x$ magnetic layer (002)-plane, respectively. As shown in Fig. 2(c), the total cross section of the layered structure and, most importantly, the columnar type growth of magnetic layer can be seen. It is shown in Figs. 2(d)–2(e) that the high magnification image of the magnetic layer reveals a high degree of crystallinity and orientation of the $c$-plane. And figure 2(f) for B8.7 film reveals the mixing of crystal and amorphous regions. Moreover, these doped elements or oxides atoms may replace Co atoms in CoIr phase or reside at the interstitial site or fill at the interspace between individual grains, which usually leads to lattice distortion and refined crystallite grains.

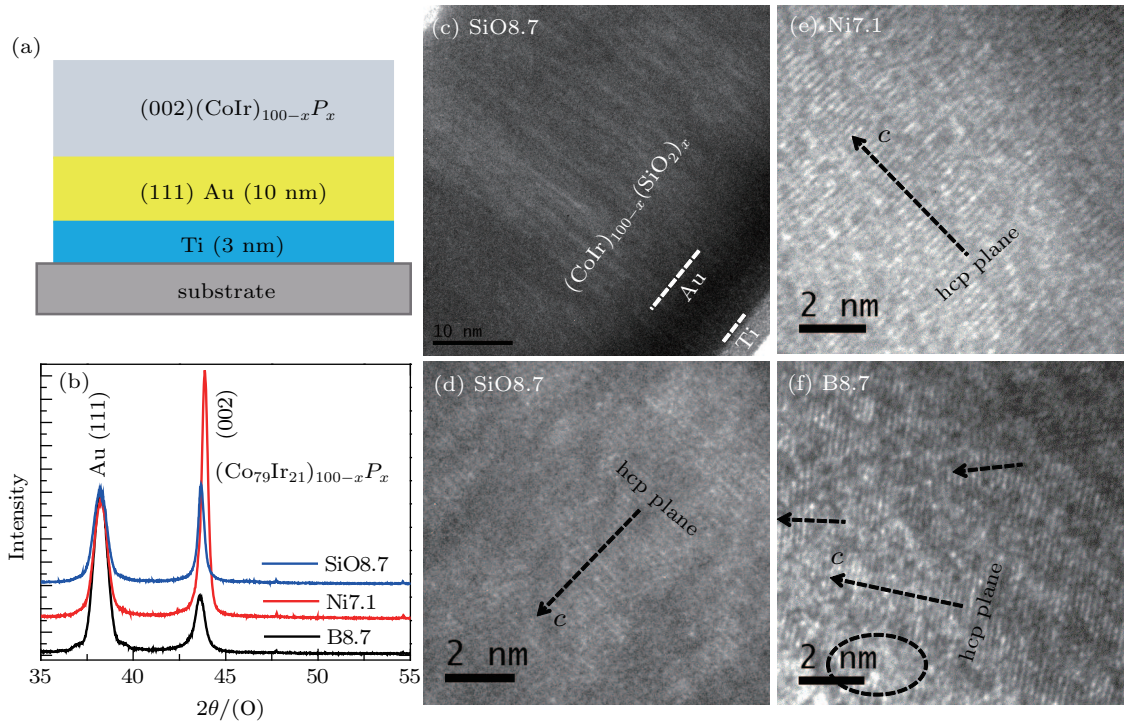



**Fig. 2.** (a) The layer structure of the $(CoIr)_{100-x}P_x$ systems and (b) the XRD patterns for SiO8.7, Ni7.1, and B8.7 films. (c) The typical transmission electron microscopy (TEM) image showing the columnar type growth of magnetic layer. (d) and (f) The high resolution imaging of the magnetic layer revealing the degree of $c$-axis orientation.

Typical in-plane magnetic hysteresis loops for sample B8.7, Ni5.3, and SiO8.7 are shown in Figs. 3(a), 3(b), and 3(c), respectively. The difference between the hysteresis loops measured along the easy axis and along the hard axis is obvious, suggesting that the samples are provided with an in-plane uniaxial anisotropy. Induced by the oblique deposition technique, the uniaxial anisotropy can be explained with the framework of the so-called self-shadowing model.[22] As shown in Fig. 3(d), the saturation magnetization $4\pi M_s$ increases gradually as the Ni contents increase, and decreases as the B and $SiO_2$ contents increase. The linear trend is similar to what was reported for FeGaB,[23] indicating the successful addition of the $P$ contents in our films.

To get $H_u$ and $K_{grain}$, we measure the resonance frequency $f_r$ by vector network analyzer (VNA) with applied field along the easy axis. As shown in Figs. 4(a)–4(c), the square of the obtained $f_r$ has a linear relationship with $H_{app}$.[24] A reasonable agreement between the experimental data and numerical fitting can be obtained. Consequently, $H_u$ and $H_\theta$ can be estimated from intercept and slope of the fitting line. The extracted $H_u$, $H_\theta$, and corresponding $K_{grain}$ are shown in Figs. 4(d), 4(e), and 4(f), respectively. First, $H_u$ changes

slightly around 30 Oe except for the maximum B doped sample B10.8 which reaches about 165 Oe. The reason may come from the strong strain and misalignment of the *c*-axis of the hcp-type grains at higher B doping.[23,25] Second, $H_\theta$ decreases with *P*-doping for all three systems increasing. Third, the calculated $K_{\rm grain}$ increases gradually with $x$ increasing, which can be explained by the lattice distortion induced orbital selective behavior of the CoIr*P* grains and the appearance of amorphous regions.[26,27] Fortunately, below about $x = 8$, our films still possess the required negative magnetocrystalline anisotropy.

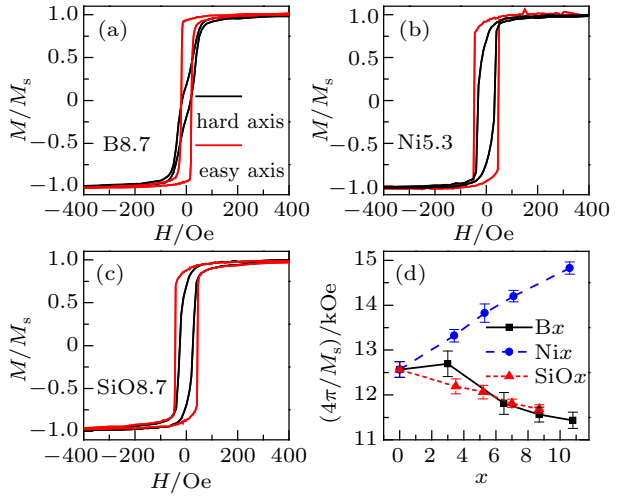



**Fig. 3.** (a)–(c) In-plane hysteresis loops measured with the external magnetic field applied along the easy axis and hard axis for sample B8.7, Ni5.3, and SiO8.7. (d) The saturation magnetization $4\pi M_{\rm s}$ determined for all the films as a function of doping level $x$.

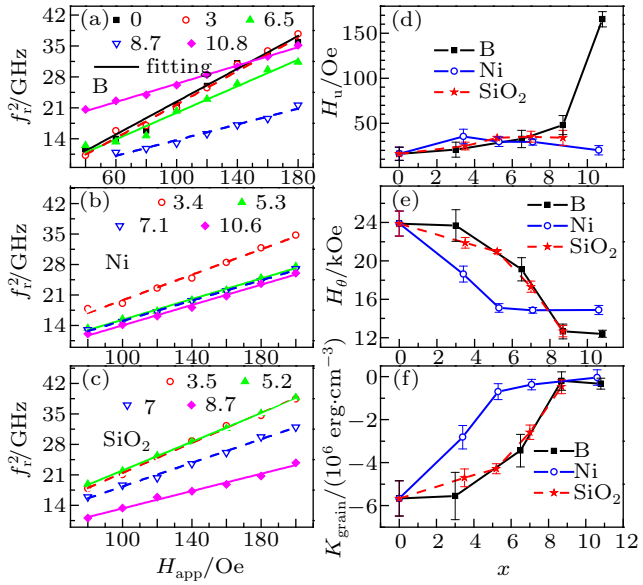



**Fig. 4.** (a)–(c) Numerical fitting of the linear relation between the applied magnetic field $H_{\rm app}$ and the square of the resonance frequency $f_{\rm r}$. (d) The determined effective in-plane anisotropy field $H_{\rm u}$, (e) the total effective out-of-plane anisotropy field $H_\theta$, and (f) the magnetocrystalline anisotropy constant $K_{\rm grain}$ as a function of $x$.

To understand and control the damping constant for practical applications, we measure the typical FMR absorption derivative profiles as shown in Figs. 5(a), 5(b), and 5(c) for samples B8.7, Ni5.3, and SiO8.7, respectively. The resonance profiles are reasonably sharp and symmetric and the Gaussian and Lorentzian profiles are used to fit the experimental data. Clearly, for all three systems, Lorentzian fits give better results and $\Delta H$ values are easily determined. This means that the intrinsic relaxation process, which can be described by the LLG equation, is the main contribution to the FMR linewidth.[28,29] It is known that the local FMR absorption profiles will spread out in the applied FMR field due to inhomogeneities. If the spreading follows Gaussian distribution, then the superposition of all local absorption profiles will show Gaussian shape to the lowest order and this will broaden the observed FMR spectrum. Therefore, the measured absorption profiles should be a superposition of Gaussian profile associated with inhomogeneities and Lorentzian profile associated with the relaxation process.[30,31] In Eq. (5), the intrinsic contribution and $\Delta\phi_{\rm u}$ contribution to the FMR linewidth will be considered. In addition, $\Delta H(0)$ plays a minor role in determining the spectral linewidth and can be ignored to some extent. For example, the reported value is about 0.1 mT in polycrystalline FeTiN films and less than 0.3 mT in yttrium iron garnet nanometer films.[28,29]

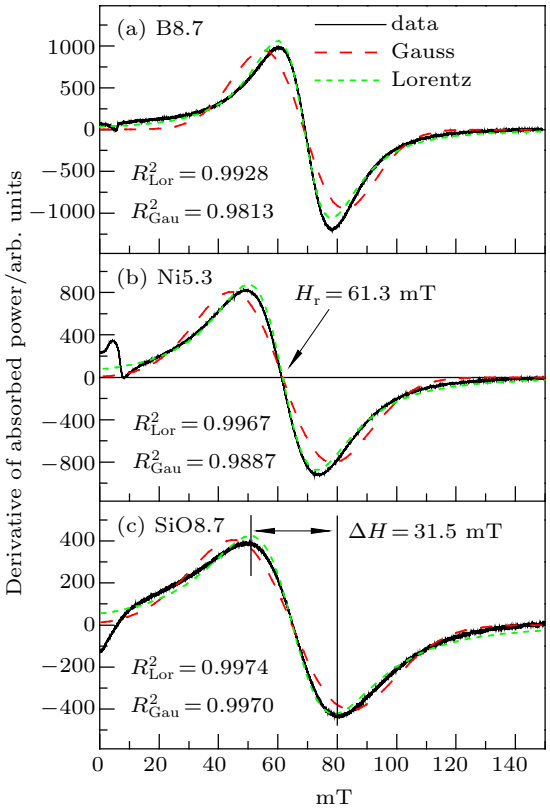



**Fig. 5.** (a)–(c) Typical FMR spectra for films B8.7, Ni5.3, and SiO8.7, respectively. The green dotted line and red dashed curve are Gaussian and Lorentzian fits to the data, respectively.

According to this discussion, the damping constants affected by the doping are thoroughly investigated. The

linewidths deduced for B$x$ as a function of the field orientation are displayed in Figs. 6(a)–6(e). The black solid lines are numerical fits to the experimental data with Eq. (7). Obviously, this model can only partly match with the experimental data. Other factors such as mosaicity as well as two-magnon scattering process[32,33] should be considered in the future to get better matching between theory and experiments. However, the average in-plane linewidth $\overline{\Delta H}$ shown in Fig. 6(f) as open black squares has the same trend with the fitted value $\Delta H_{\rm e}^{\rm fit}$ which is mainly ascribed to the intrinsic Gilbert damping when the external magnetic field is applied either along the easy or along the hard axis.[33] A similar tendency suggests that the change in $\Delta H$ is mainly caused by the variation of the intrinsic Gilbert damping. The extracted $\alpha$ plotted as a function of $x$ in Fig. 6(g) has the decreasing tendency as the B content increases. The $\Delta\phi_{\rm u}$ shown in Fig. 6(h) does not change much with $x$. The only small reduction of $\Delta\phi_{\rm u}$ might be associated with misfit and/or dislocations resulting from defects and/or internal stress.[34]

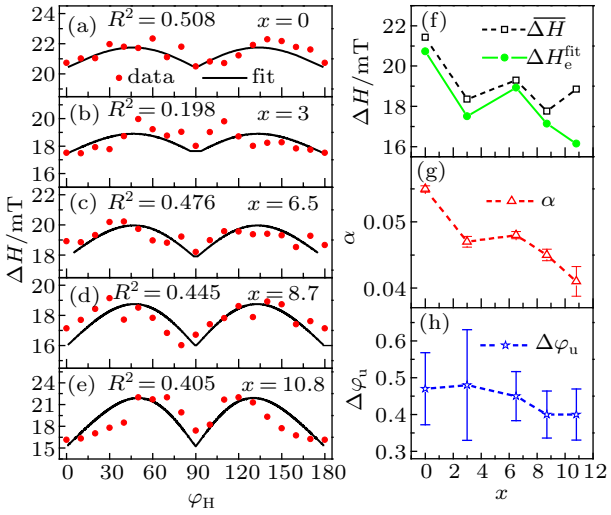



**Fig. 6.** (a)–(e) The angle dependence of the linewidth $\Delta H$ for the oriented hcp-$(CoIr)_{100-x}B_x$ films, (f) the $\Delta H_{\rm e}^{\rm fit}$ and average in-plane linewidth $\overline{\Delta H}$, and (g) the damping constant $\alpha$. (h) The angular spreading of the uniaxial field $\Delta\phi_{\rm u}$ as a function of $x$.

For Ni$x$ films, figures 7(a)–7(e) show the linewidth as a function of the field orientation. The fitted results are plotted in Figs. 7(f)–7(h) as a function of $x$. As $x$ increases, both $\overline{\Delta H}$ and $\Delta H_{\rm e}^{\rm fit}$ show approximately the same value and an oscillating behavior. The same trend suggests again that the change in $\Delta H$ is mainly caused by the variation of the intrinsic Gilbert damping. The same behavior is also observed for $\alpha$ as shown in Fig. 7(g). The $\Delta\phi_{\rm u}$ shows a decrease with increasing $x$, similar to the B$x$ system.

The same analysis procedures have been done for the SiO$x$ samples, as shown in Figs. 8(a)–8(e). As seen from Figs. 8(f)–8(h), the values of $\overline{\Delta H}$ and $\Delta H_{\rm e}^{\rm fit}$ first show a slow decrease and then faster increase with $x$, which suggests an intrinsic Gilbert damping. The change of $\alpha$ with $x$ is also similar to the change of $\overline{\Delta H}$, and $\Delta\phi_{\rm u}$ shows a small decrease with increasing $x$.

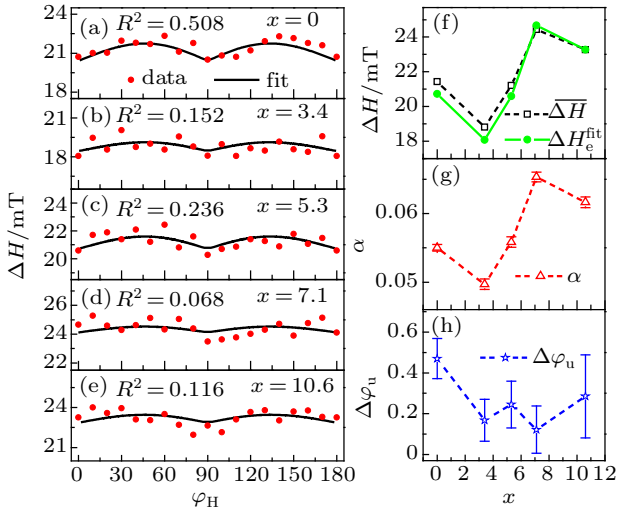



**Fig. 7.** (a)–(e) The angle dependence of the linewidth $\Delta H$ for the oriented hcp-$(CoIr)_{100-x}Ni_x$ films. (f) The $\Delta H_{\rm e}^{\rm fit}$ and average in-plane linewidth $\overline{\Delta H}$, (g) the damping constant $\alpha$, and (h) the angular spreading of the uniaxial field $\Delta\phi_{\rm u}$ as a function of $x$.

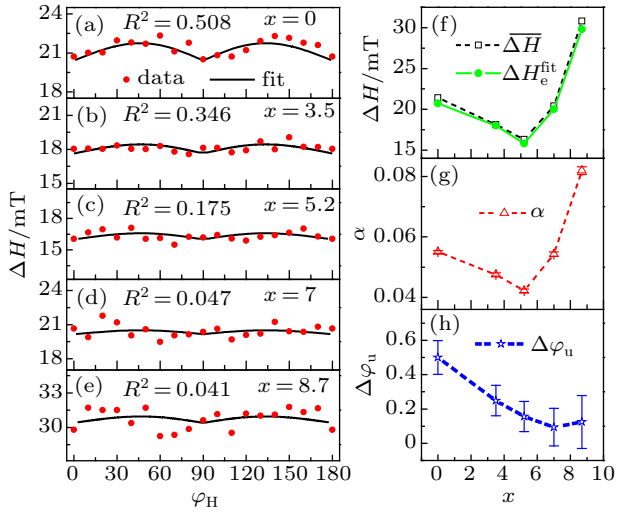



**Fig. 8.** (a)–(e) The angle dependence of the linewidth $\Delta H$ for the films with $SiO_2$ addition. (f) The $\Delta H_{\rm e}^{\rm fit}$ and average in-plane linewidth $\overline{\Delta H}$, (g) the damping constant $\alpha$, and (h) The angular spreading of the uniaxial field $\Delta\phi_{\rm u}$ as a function of $x$.

For better comparison, we summarize our results of the damping constant in Fig. 9. Although the intrinsic part largely depends on spin–orbit coupling effect, the magnetic damping mechanism in ferromagnetic materials has not been clarified so far.[35] However, in practical application, the damping constant can be controlled by using the method of doping the third content into the material. For clarity, the data are normalized to the initial value with zero doping. Obviously, $SiO_2$-doping is more effective in tuning the damping constant for the CoIr film.

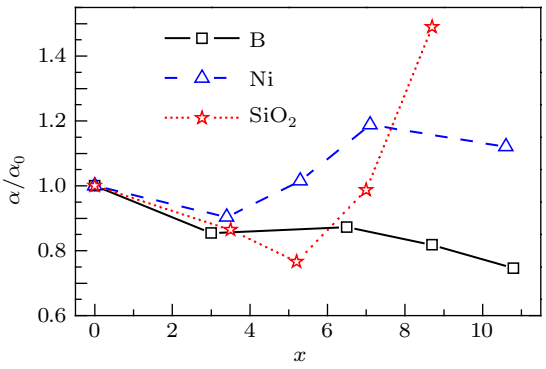



**Fig. 9.** The normalized damping constant $\alpha$ for all samples as a function of $x$.

## 5. Conclusion

In summary, soft magnetic thin films of $(CoIr)_{100-x}P_x$ ($P$ = B, Ni, and $SiO_2$) have been fabricated by DC magnetron sputtering. As $x$ increases, the saturation magnetization decreases gradually for B and $SiO_2$ doping, while it increases with $x$ for Ni doping. The measured absorption profiles consist of mainly the Lorentzian profile associated with the intrinsic relaxation process. The experimental angular dependence of $\Delta H$ is numerically analyzed based on the LLG equation. The change of $\Delta H$ is mainly caused by the variation of the intrinsic Gilbert damping, while the $\Delta\phi_u$ part originating from inhomogeneities only plays a minor role. The extracted $\alpha$ and $\Delta\phi_u$ are thoroughly investigated as a function of $x$ and our results show that the damping constant can be controlled by doping the third content into the materials of interest.

## References


[1] Kalarickal S S, Krivosik P, Das J, Kim K S and Patton C E 2008 *Phys. Rev. B* **77** 054427
[2] Fassbender J, von Borany J, Mücklich A, Potzger K and Möller W 2006 *Phys. Rev. B* **73** 184410
[3] Fujita N, Inaba N, Kirino F, Igarashi S, Koike K and Kato H 2008 *J. Magn. Magn. Mater.* **320** 3019
[4] Guo X B, Xi L, Li Y, Han X M, Li D, Wang Z and Zuo Y L 2014 *Appl. Phys. Lett.* **105** 072411
[5] Sun N X and Wang S X 2000 *IEEE Trans. Magn.* **36** 2506
[6] Kambersky V 1970 *Can. J. Phys. B* **48** 2906
[7] Arias R and Mills D L 1999 *Phys. Rev. B* **60** 7395
[8] Chappert C, Dang K L, Beauvillain P, Hurdequint H and Renard D 1986 *Phys. Rev. B* **34** 3192
[9] Ingvarsson S, Xiao G, Parkin S S P and Koch R H 2004 *Appl. Phys. Lett.* **85.** 4995
[10] Zhang Z, Lin M, Zhu J, Guo D, Chai G, Fan X, Yang Y and Xue D 2010 *J. Appl. Phys.* **107** 083912
[11] Rantschler J O, McMichael R D, Castillo A, Shapiro A J, Egelhoff W F, Maranville B B, Pulugurtha D, Chen A P and Connors L M 2007 *J. Appl. Phys.* **101** 033911
[12] Fassbender J, Borany J, Mücklich A, Potzger K, Möller W, McCord J and Schultz L 2006 *Phys. Rev. B* **73** 184410
[13] Ma T Y, Jiao J Y, Li Z W, Qiao L, Wang T and Li F S 2017 *J. Magn. Magn. Mater.* **444** 119
[14] Hashimoto A, Saito S and Takahashi M 2006 *J. Appl. Phys.* **99** 08Q907
[15] Xu F, Wang T, Ma T Y, Wang Y, Zhu S M and Li F S 2016 *Sci. Rep.* **6** 20140
[16] Wang T, Wang Y, Tan G G, Li F S and Ishio S 2013 *Physica B* **417** 24
[17] Wong H S, He S K, Chung H J, Zhang M S, Cher K, Low M, Zhou T J, Yang Y and Wong S K 2016 *Nanotechnology* **27** 455705
[18] Hashimoto A, Saito S and Takahashi M 2006 *J. Magn. Soc. Jpn.* **30** 135
[19] Takahashi M, Tsunoda M and Saito S 2009 *ECS Trans.* **16** 19
[20] Manuilov S A, Grishin A M and Munakata M 2011 *J. Appl. Phys.* **109** 083926
[21] Yuan S J, Kang B J, Yu L M, Cao S X and Zhao X L 2009 *J. Appl. Phys.* **105** 063902
[22] Xue D S, Fan X L and Jiang C J 2006 *Appl. Phys. Lett.* **89** 011910
[23] Lou J, Insignares R E, Cai Z, Ziemer K S, Liu M and Sun N X 2007 *Appl. Phys. Lett.* **91** 182504
[24] Cao D R, Cheng X H, Feng H M, Jin C D, Zhu Z T, Pan L N, Wang Z K, Wang J B and Liu Q F 2016 *J. Alloys Compd.* **688** 917
[25] Munakata M, Aoqui S and Yagi M 2005 *IEEE Trans. Magn.* **41** 3262
[26] Trygg J, Johansson B, Eriksson O and Wills J M 1995 *Phys. Rev. Lett.* **75** 2871
[27] Daalderop G H O, Kelly P J and Schuurmans M F H 1990 *Phys. Rev. B* **41** 11919
[28] Liu T, Chang H, Vlaminck V, Vlaminck V, Sun Y, Kabatek M, Hoffmann A, Deng L J and Wu M Z 2014 *J. App. Phys.* **115** 17A501
[29] Kalarickal S S, Krivosik P, Das J, Kim K S and Patton C E 2008 *Phys. Rev. B* **77** 054427
[30] Heinrich B, Urban R and Woltersdorf G 2002 *J. App. Phys.* **91** 7523
[31] Mizukami S, Ando Y and Miyazaki T 2002 *Phys. Rev. B* **66** 104413
[32] Arias R and Mills D L 1999 *Phys. Rev. B* **60** 7395
[33] Chappert C, Dang K L, Beauvillain P, Hurdequint H and Renard D 1986 *Phys. Rev. B* **34** 3192
[34] Fermin J R, Azevedo A, de Aguiar F M, Li B and Rezende S M 1999 *J. App. Phys.* **85** 7316
[35] Pelzl J, Meckenstock R, Spoddig D, Schreiber F, Pflaum J and Frait Z 2003 *Condens. Matter* **15** S451